AgFeS$_2$-Nanowire-Modified BiVO$_4$ Photoanodes for Photoelectrochemical Water Splitting

Xiuzhen Zheng,[a] Beniamino Sciacca,[b] Erik C. Garnett,*[b] and Liwu Zhang*[a]

Photoelectrochemical water splitting is a promising and environmentally friendly route for the conversion of solar energy into hydrogen. However, the efficiency of this energy conversion process is low because of the limited light absorption and rapid bulk recombination of charge carriers. In this study, the combination of a novel ternary sensitizer AgFeS$_2$, having a narrow bandgap of 0.9 eV, with a BiVO$_4$ electrode is presented for the enhancement of the solar-energy-to-hydrogen conversion efficiency. The photoelectrochemical properties of this combined material were investigated and the photocurrent densities of AgFeS$_2$–BiVO$_4$ composite electrodes were greatly enhanced compared with pristine BiVO$_4$ (15 times higher at 0.6 V vs. Ag/AgCl under AM 1.5G illumination). The enhanced photoelectrochemical properties arise from extended light absorption, fast charge transfer and appropriate energy gap alignment. It was demonstrated that AgFeS$_2$ nanowires are promising inorganic sensitizers for improving the efficiency of solar water splitting.

Introduction

Since the discovery of water splitting on titanium dioxide (TiO$_2$) surfaces by photoirradiation, photoelectrochemical (PEC) technology has attracted extensive interest.[1] After decades of development, great progress has been made in the production of H$_2$ by water splitting, the degradation of organic pollutants and CO$_2$ reduction.[2–5] However, the efficiency of such PEC processes is still low, which seriously restricts their wide application in solving energy shortage and environmental pollution problems. Investigating new and efficient photoelectrodes has been shown to be important for improving PEC efficiency and promoting the practical application of PEC technology. Among photoelectrode materials, bismuth vanadate (BiVO$_4$) is one of the leading metal oxides, with a direct bandgap of 2.3–2.4 eV and a suitable valence band position for O$_2$ evolution.[6] BiVO$_4$ was first reported by Kudo and co-workers as a photocatalyst for water oxidation.[7] Since then, BiVO$_4$ has been widely investigated as a visible-light-driven photocatalyst for water oxidation and organic compound degradation.[8–12] Recently, extensive attention has focused on BiVO$_4$ as a photoanode for PEC water splitting.[13–16] However, the activity of pure BiVO$_4$ is low due to its poor light absorption and difficult migration of electron–hole pairs, which has been demonstrated by van de Krol and co-workers.[17] Therefore, poor electron transport results in high bulk recombination of photogenerated charge carriers and low solar-to-hydrogen energy conversion efficiency.

To address these issues, many attempts have been made to modify the bulk electronic properties of BiVO$_4$ photocatalysts, such as applying noble-metal coatings, elemental doping and combining narrow bandgap semiconductors.[15,18–23] Among these methods, one of the most efficient ways is to deposit a sensitizer with an appropriate band gap onto BiVO$_4$. The sensitizer not only extends the light absorption spectrum, but also accelerates photogenerated electron–hole separation. Ternary I–III–VI$_2$ semiconductors are regarded as one of the most promising materials for thin-film sensitizers because of their unique properties, large absorption coefficients, high conversion efficiency, and low toxicity.[24] Silver iron sulfide (AgFeS$_2$, Lenaite) is a novel ternary I–III–VI$_2$ semiconductor, which has a narrow band gap ($\approx$0.9 eV) covering the entire visible spectrum and also has a high absorption coefficient.[25] Sciacca et al. and Han et al. have obtained AgFeS$_2$ by different synthetic pathways.[25,26] To the best of our knowledge, to date, there has been no report on PEC electrodes made from BiVO$_4$ modified with ternary AgFeS$_2$. This study extends the work to a new, coupled photoanode consisting of the ternary sensitizer AgFeS$_2$ and BiVO$_4$.

We prepared a AgFeS$_2$–BiVO$_4$ composite by incorporating AgFeS$_2$ with a BiVO$_4$ film by means of a simple drop-coating method. The composite of AgFeS$_2$ and BiVO$_4$ semiconductors with appropriate oxidation–reduction energy levels enhanced the charge separation and generated a wide spectral response by extension of light absorption in the visible region. In this study, ternary AgFeS$_2$-modified BiVO$_4$ is fabricated on a fluorine-doped tin oxide (FTO) substrate and applied as a photoa-

[a] *Dr. X. Zheng, Prof. L. Zhang*
Shanghai Key Laboratory of Atmospheric Particle Pollution and Prevention
Department of Environmental Science and Engineering
Fudan University, Shanghai 200433 (P. R. China)
E-mail: zhanglw@fudan.edu.cn

[b] *Dr. B. Sciacca, Dr. E. C. Garnett*
Center for Nanophotonics, FOM Institute AMOLF
Science Park Amsterdam 104
1098 XG Amsterdam (The Netherlands)
E-mail: e.garnett@amolf.nl

Supporting information for this article can be found under http://dx.doi.org/10.1002/cplu.201600095.

This article is part of a Special Issue on "Catalytic Systems for Water Splitting". To view the complete issue, visit: http://dx.doi.org/10.1002/cplu.v81.10.

node. The expected enhanced PEC properties of AgFeS$_2$–BiVO$_4$ composite were confirmed by hydrogen and oxygen evolution from solar water splitting. The mechanism for the enhanced PEC performance and gas evolution on the AgFeS$_2$–BiVO$_4$ composite is discussed in detail.

Results and Discussion

Fabrication and characterization of AgFeS$_2$–BiVO$_4$ composite electrodes

Scanning electron microscopy (SEM) was used to investigate the morphology of the as-prepared AgFeS$_2$, BiVO$_4$ and AgFeS$_2$–BiVO$_4$ samples (Figure 1). Figure 1a shows the typical morphol-
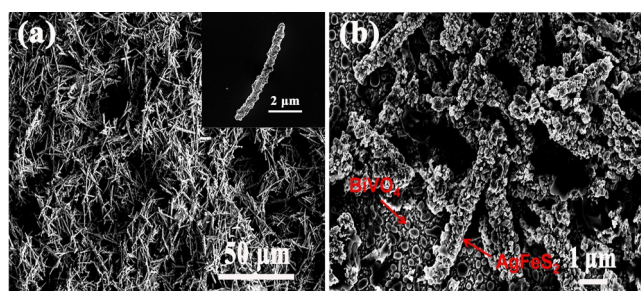
Figure 1. SEM images of a) AgFeS$_2$ nanowires and b) AB-40 composite.

ogy of AgFeS$_2$. It is comprised of nanowires approximately 10 μm in length. The morphology of the BiVO$_4$ (Figure S1 in the Supporting information) was also investigated, and was found to comprise nanoparticles with diameters from 100 to 400 nm. AgFeS$_2$ nanowires were firstly prepared by a solution-phase conversion of metallic Ag nanowires described in our previous report.[25] The as-prepared AgFeS$_2$ nanowires were then stirred in ethanol for 24 h to form a suspension, which was dropped onto the BiVO$_4$ film to obtain the AgFeS$_2$–BiVO$_4$ composite. According to the amount of AgFeS$_2$ (10, 20, 30, 40 and 50 μL) being added on the BiVO$_4$ samples, the corresponding AgFeS$_2$–BiVO$_4$ samples were designated AB-10, AB-20, AB-30, AB-40 and AB-50, respectively. As the morphologies of AgFeS$_2$–BiVO$_4$ samples containing different amounts of AgFeS$_2$ are almost the same, only the coverage of AgFeS$_2$ on BiVO$_4$ is different. The photocurrent density of the AB-40 electrode is higher than other AgFeS$_2$–BiVO$_4$ samples, therefore it was chosen as the example composite for the SEM and energy-dispersive X-ray (EDX) measurements. For the AB-40 sample, it was clearly observed that AgFeS$_2$ nanowires are on the top surface of BiVO$_4$ (Figure 1b and Figure S2). Furthermore, EDX mapping obtained in the SEM mode (Figure 2) was performed to confirm the composition of AB-40. As seen from the SEM image (Figure 2a), the AgFeS$_2$ nanowires are crystalline, which was confirmed by electron diffraction in our previous synthetic study.[25] Moreover, the elements Ag, Fe, and S (Figure 2b–d) are distributed homogeneously along the nanowires, indicating the existence of AgFeS$_2$. The elements Bi, V and O (Figure 2e–g) were also detected, which are associated with the
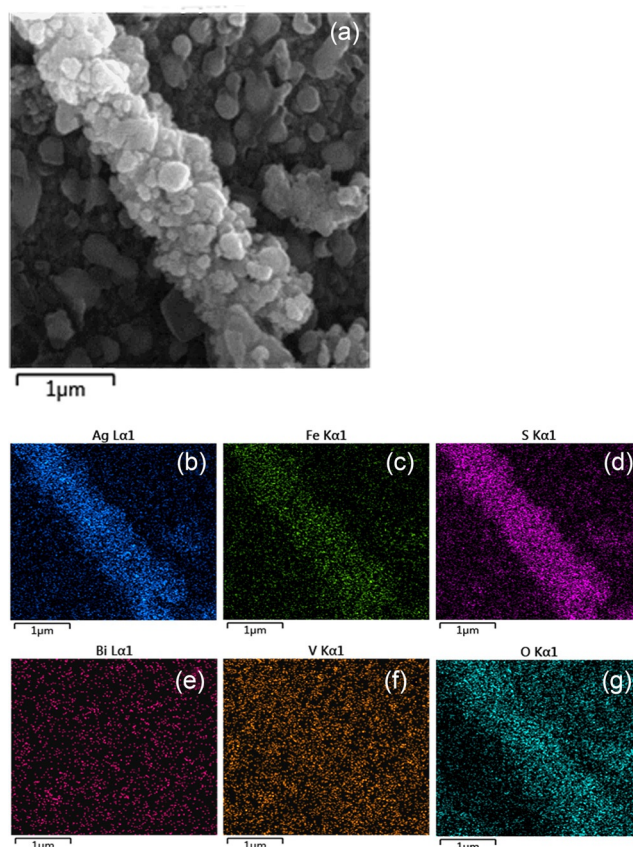
Figure 2. SEM and EDX characterization of AB-40 sample: a) high-magnification SEM image; b–g) element mapping of Ag, Fe, S, Bi, V and O, respectively.

BiVO$_4$ substrate. The composite structure of AgFeS$_2$–BiVO$_4$ was thus confirmed by the SEM and EDX results.

The crystal structures of BiVO$_4$ and AB-40 were determined by x-ray diffraction (XRD), as shown in Figure 3. The XRD pattern of BiVO$_4$ can be matched to monoclinic BiVO$_4$ (JCPDS No. 14-0688); the FTO film (JCPDS No. 41-1445) is shown in Figure S3. The 2θ diffraction peaks of 28.8°, 30.5°, 34.5°, 35.2°, 39.8°, and 42.5° can be respectively indexed as the (121), (040),
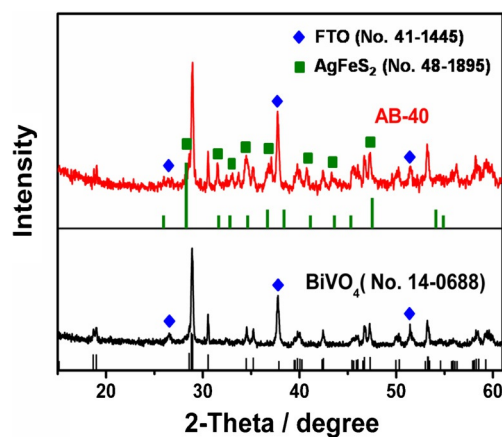
Figure 3. XRD patterns of BiVO$_4$ and AB-40.

(200), (002), (211), and (051) planes of the monoclinic $BiVO_4$ structure, which is consistent with the literature.[27] The 2θ diffraction peaks and corresponding planes of $AgFeS_2$ (JCPDS No. 48-1895) are shown in Figure S4. Notably, $AgFeS_2$ is clearly apparent in the XRD pattern of the AB-40 sample. Based on the results of SEM images, elemental mapping and XRD patterns, it is clear that the $AgFeS_2$–$BiVO_4$ composite was successfully prepared using a simple drop-coating approach.

It is well known that light absorption of the photoelectrode material plays an important role in solar water splitting. The UV/Vis diffuse reflection spectra of $BiVO_4$, $AgFeS_2$, and $AgFeS_2$–$BiVO_4$ composites with different $AgFeS_2$ content were thus measured. The optical bandgap energy (E_g) of $BiVO_4$ (Figure S5) was obtained by using the equation $[F(R)E]^{1/2} = A(E-E_g)$.[28] where E is the energy of a photon and A is a constant. The estimated bandgap value of $BiVO_4$ as a direct band semiconductor is 2.32 eV, which is in agreement with previously reported values.[7,8] From a further analysis of the diffuse reflection spectra (Figure 4), it is apparent that there are enhancements in
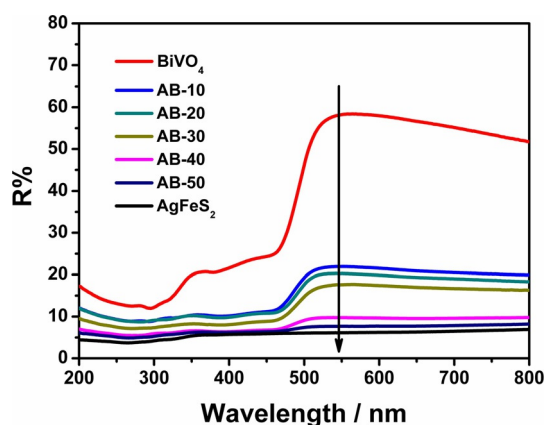
Figure 4. UV/Vis diffuse reflectance spectra of $AgFeS_2$, $BiVO_4$ and $AgFeS_2$–$BiVO_4$ composites with different $AgFeS_2$ contents.

the light absorption of $AgFeS_2$–$BiVO_4$ composites compared with the bare $BiVO_4$. This is due to the fact that $AgFeS_2$, having a narrow band gap (0.88 eV), significantly extends the light absorption range of $AgFeS_2$–$BiVO_4$ composites. With the introduction of $AgFeS_2$, a more efficient utilization of the solar spectrum on $AgFeS_2$–$BiVO_4$ can be achieved, which is helpful to improve the PEC properties and facilitates its use in practical solar water splitting. The $AgFeS_2$–FTO film was prepared by adding a $AgFeS_2$ suspension onto FTO until fully covering the surface. Therefore, the amount of $AgFeS_2$ on the FTO substrate is higher than the other samples; this is the reason that $AgFeS_2$ film has much lower $R\%$ (reflectance).

Photoelectrochemical properties of $AgFeS_2$–$BiVO_4$ electrodes

The photocurrent densities as a function of applied potential of $AgFeS_2$, $BiVO_4$ and $AgFeS_2$–$BiVO_4$ electrodes were investigated by linear sweep photovoltammetry (LSV), which measured

their electron generation capacity and electron transfer efficiency. The photocurrent responses of $AgFeS_2$, $BiVO_4$ and $AgFeS_2$–$BiVO_4$ photoelectrodes (Figure 5) were studied under AM 1.5G illumination (100 mW cm^{-2}). Figure 5a shows LSV (scan rate 10 mV s^{-1}) of the $BiVO_4$, $AgFeS_2$ and $AgFeS_2$–$BiVO_4$ photoanodes under illumination from the backside (FTO side) of the electrodes. The anodic photocurrents increased steadily with the applied positive potential, and an enhanced photocurrent for the $AgFeS_2$–$BiVO_4$ composite electrodes was obtained essentially over the entire potential range compared with $BiVO_4$ electrode. The AB-40 electrode showed the greatest enhancement of all of the electrodes, and the current in the dark was negligible. This significant improvement in photocurrent could be attributed to the effect of $AgFeS_2$ modification. It is also notable that pristine $AgFeS_2$ shows a low photocurrent. The linear sweep voltammograms of the photoanodes under chopped illumination were also studied and showed a similar trend (Figure 5b). The $BiVO_4$ photoanode demonstrated a low photocurrent that is indeed lower than most of the values reported in the literature on $BiVO_4$ photoelectrodes.[29,30] The poor PEC performance is mainly caused by non-uniform distribution of the $BiVO_4$ nanoparticles on the FTO surface, which is not fully covered by $BiVO_4$ nanoparticles. It was thus anticipated that the photocurrent of the $AgFeS_2$–$BiVO_4$ composite
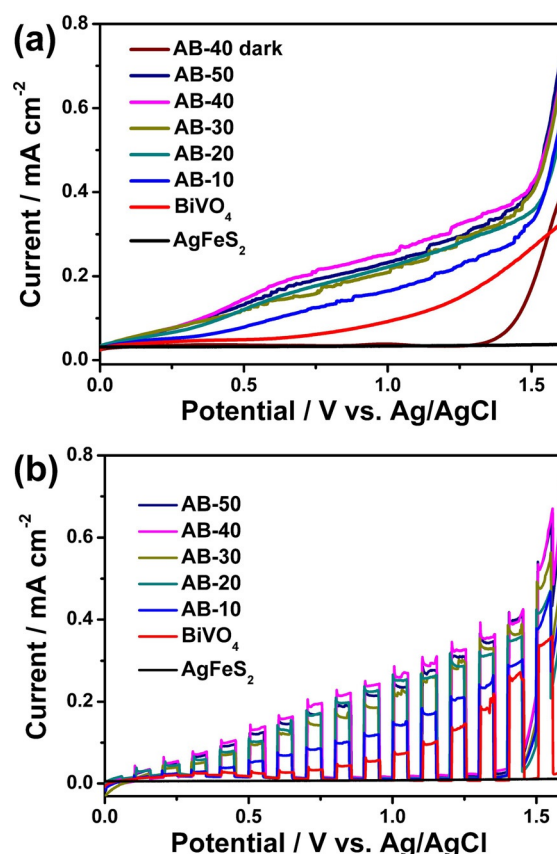
Figure 5. Photocurrent generation versus bias potential (vs. Ag/AgCl) obtained from $AgFeS_2$, $BiVO_4$ and $AgFeS_2$–$BiVO_4$ composites a) without chopped illumination and b) under chopped AM 1.5G illumination (100 mW cm^{-2}) in 0.1 M Na_2SO_4.

would be much higher if a $BiVO_4$ substrate of better quality was used.

Additional PEC measurements (Figure 6) were performed to further investigate the enhancement mechanism for water splitting at the $AgFeS_2$–$BiVO_4$ composite electrode. Figure 6a shows the photocurrent versus time curves (0.6 V vs. Ag/AgCl under AM 1.5G illumination) for the samples with several on–off cycles. The photocurrent responses of the $AgFeS_2$–$BiVO_4$ composite films were higher than those of $BiVO_4$ and $AgFeS_2$, and AB-40 demonstrated the highest photocurrent among them, which was almost 15 times higher than that of $BiVO_4$. As shown in Figure 6b, it is clear that the radius of the arc on the electrochemical impedance spectroscopy (EIS) Nyquist plots of $AgFeS_2$–$BiVO_4$ samples are smaller than that of $BiVO_4$, which is consistent with $AgFeS_2$–$BiVO_4$ favoring faster interfacial charge transfer. The results are in good agreement with the photocurrent measurements. According to the photocurrent curves and EIS plots, the presence of $AgFeS_2$ in the $AgFeS_2$–$BiVO_4$ composite is capable of improving separation efficiency and effectively inhibiting the recombination of photogenerated electron–hole pairs. Such an explanation would also make more sense given its small bandgap, which means it should not participate directly in water splitting.

To further gain a qualitative understanding of the charge recombination behavior in $BiVO_4$ and AB-40, the transient photocurrent decay occurring immediately upon illumination was investigated (Figure 6c). Measuring the transient photocurrent response has been demonstrated to be a useful technique for investigating the efficiency of the separation of photogenerated electron–hole pairs.[31] The photocurrent curve initially presents a spike, which gradually decays until the photocurrent reaches a stable value. The decrease in the photocurrent indicates that recombination occurs within the $AgFeS_2$–$BiVO_4$ electrode. If the incident light is switched on, a photocurrent spike is observed at an applied potential of 0.6 V versus Ag/AgCl due to the sudden generation of charge carriers, which then recombine. Charge recombination can be caused either by accumulation of electrons in the bulk or accumulation of holes at the surface. The accumulation of holes would cause an equally large cathodic transient if the light is switched off and electrons in the conduction band react with the accumulated holes.[9] However, cathodic transients were barely observed, indicating that accumulation of holes is not the main recombination process in $BiVO_4$ film and AB-40 electrodes. The transients shown in Figure 6c are thus attributed to the accumulation of electrons due to the poor electron transport in $BiVO_4$, which is
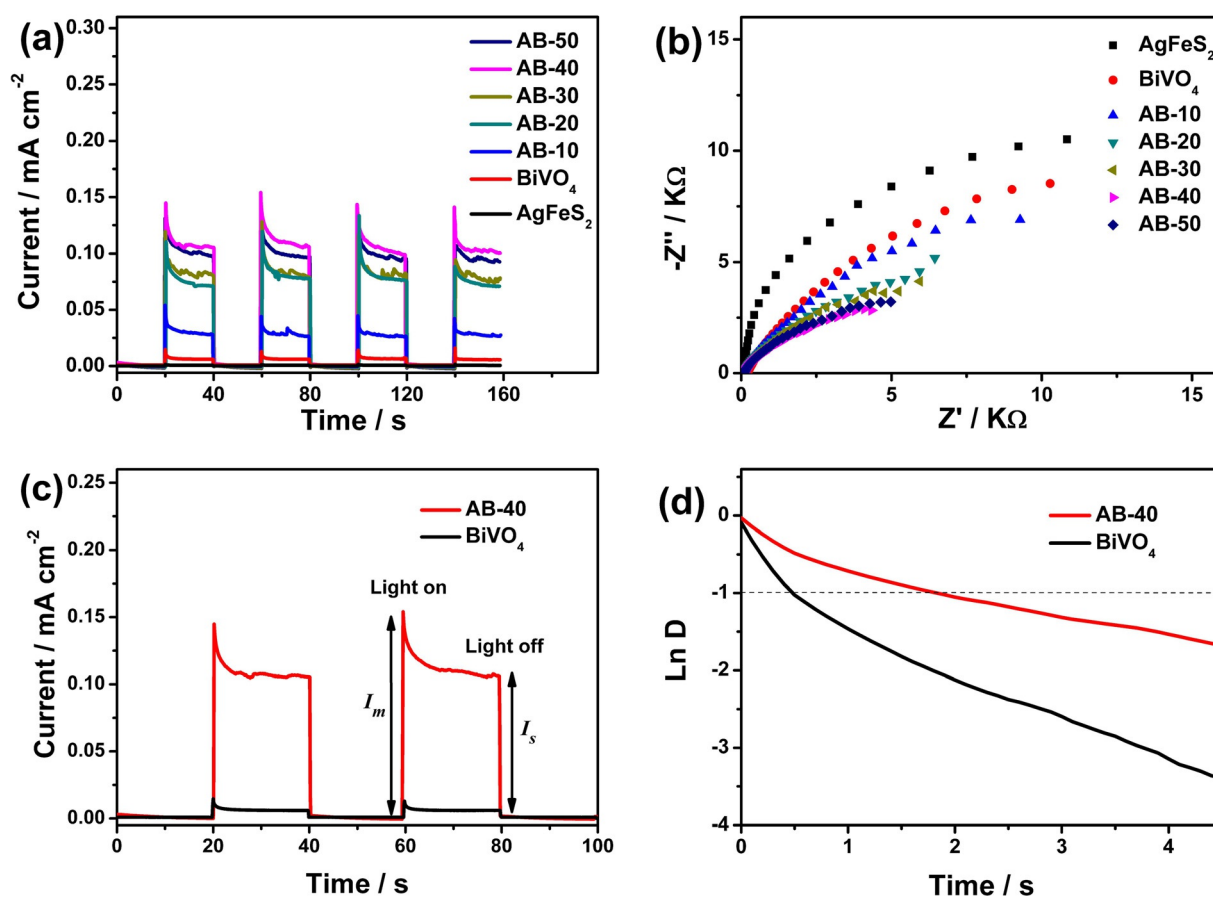
Figure 6. a) Photocurrent spectra and b) EIS Nyquist plots of $AgFeS_2$, $BiVO_4$ and $AgFeS_2$–$BiVO_4$ with an applied bias potential of 0.6 V vs. Ag/AgCl under AM 1.5G illumination (100 mW cm^{-2}). c) Transient photocurrent decay and d) transient decay times of $BiVO_4$ film and AB-40 electrodes (see text for the definition of parameter D).

consistent with results observed previously.[14] The transient decay time can be calculated from a logarithmic plot of parameter D, given by Equation (1):[32,33]

$$D = (I_t - I_s)/(I_m - I_s) \tag{1}$$

where I_m is the maximum photocurrent of the spike, I_t is the photocurrent at time t and I_s is the steady-state photocurrent. I_s is achieved as the recombination and charge generation reaches equilibrium. The transient decay time is defined as the time at which $\ln D = -1$.[32] Therefore, based on the photocurrent profiles (Figure 6c), the transient decay times of BiVO$_4$ film and AB-40 electrodes were calculated and are plotted in Figure 6d. The transient decay time for AB-40 electrode was 1.87 s, which is more than three times longer than the transient decay time of BiVO$_4$ film (0.49 s). In general, the photocurrent decay rate is determined by the charge carrier recombination rate.[33] Therefore, we expect that a slower recombination rate gives rise to a longer transient decay time. Indeed, a significantly longer transient decay time was observed for the AB-40, suggesting a lower charge carrier recombination rate in AB-40 compared to the BiVO$_4$ film.

In order to address the quantitative correlation between AgFeS$_2$ sensitization and light absorption of AgFeS$_2$–BiVO$_4$ composites, incident-photon-to-current-conversion efficiency (IPCE) measurements were performed to study the photoactive wavelength regime for AgFeS$_2$, BiVO$_4$ and AB-40 (Figure 7). IPCE can be expressed as Equation (2):[34,35]

$$IPCE = (1240 \times I)/(\lambda \times J_{light}) \tag{2}$$

where I is the photocurrent density, λ is the wavelength of the incident light, and J_{light} is the measured irradiance. For AgFeS$_2$ itself, the IPCE data is low, which is consistent with the photocurrent data. The IPCE plots of BiVO$_4$ and AB-40 look similar and strongly decrease upon excitation at longer wavelengths; the BiVO$_4$ showed a minimal photoresponse below the bandgap energy ($\approx$ 2.32 eV, 535 nm), whereas the composite electrode (AB-40) showed a significant redshift toward lower
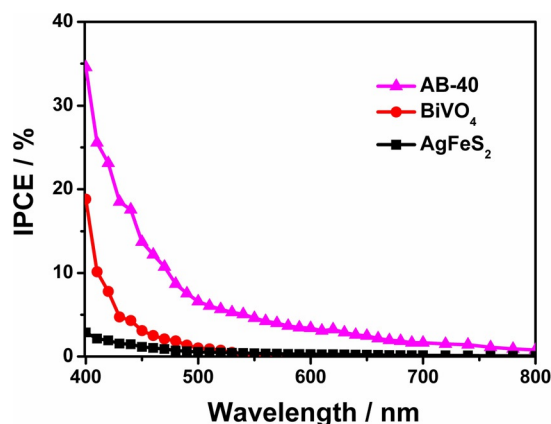
Figure 7. Measured IPCE spectra of AgFeS$_2$, BiVO$_4$ and AB-40 in the region 400–800 nm at a potential of $+0.6$ V under AM 1.5G illumination (100 mW cm^{-2}).

energy. For example, at above-bandgap illumination, the IPCE of pure BiVO$_4$ and AB-40 samples at the incident wavelength of 500 nm are 1.03 % and 6.59 %, respectively, indicating that the presence of AgFeS$_2$ can improve the charge separation efficiency and thus give an enhanced photoresponse. At below-bandgap illumination of 550 nm, the IPCE of AB-40 is around 5 %, while pristine BiVO$_4$ shows no photoresponse. This is direct evidence that AgFeS$_2$ can also act as a photosensitizer and substantially improves the light collection and conversion efficiency in the visible region.

To verify that the measured photocurrent of the photoanodes originated from water splitting and not undesired side reactions, a water splitting experiment was performed at 1.6 V on the AB-40 photoanode, and the gas evolution (Figure 8)
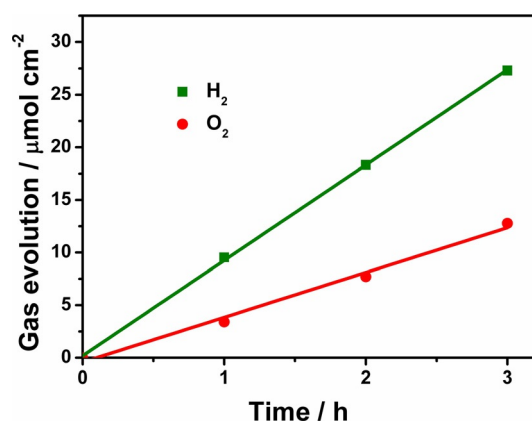
Figure 8. Gas evolution of the AB-40 photoanode at an applied potential of 1.6 V (vs. Ag/AgCl) under AM 1.5G illumination (100 mW cm^{-2}).

and corresponding photocurrent response (Figure S6) were measured. The ratio of evolution rates of H$_2$ and O$_2$ is close to the stoichiometric value of 2.0, with rates of 9.1 ± 0.1 µmol h^{-1} cm^{-2} for H$_2$ and 4.3 ± 0.1 µmol h^{-1} cm^{-2} for O$_2$. By assuming 100 % faradaic efficiency, at a photocurrent of 0.60 mA cm^{-2}, the evolution rates of H$_2$ and O$_2$ should be 10.6 and 5.3 µmol h^{-1} cm^{-2}, respectively. Hence the faradaic efficiencies for H$_2$ and O$_2$ are more than 80 %, indicating that the observed photocurrent could be mostly attributed to water splitting. Additionally, the photocurrent of AB-40 only slightly decreases after 3 h of the water splitting experiment (Figure S6), implying the high stability of the AgFeS$_2$–BiVO$_4$ composite photoanode. It can be concluded that AgFeS$_2$ is relatively stable and promising as a sensitizer for solar water splitting.

Photoelectrochemical mechanism for water splitting at the AgFeS$_2$–BiVO$_4$ composite photoanode

Based on the above data, a possible mechanism for the water splitting at the AgFeS$_2$–BiVO$_4$ composite photoanode under light irradiation can be proposed. Here AgFeS$_2$ serves as a sensitizer for light-induced redox process and BiVO$_4$ is a substrate. The bandgap of BiVO$_4$ was evaluated as 2.32 eV from the UV/Vis spectrum, which is consistent with literature reports.[7,8] The

corresponding conduction band (E_{CB}) and valence band (E_{VB}) positions of $BiVO_4$ and $AgFeS_2$ at the point of zero charge were presumed according to the following equations [Eqs. (3) and (4)]:[36,37]

$$\chi = 1/2(A_f + I_1) \qquad (3)$$

$$E_{CB} = \chi - E_0 - 1/2\,E_g \qquad (4)$$

where χ is the bulk electronegativity of the compound, defined as the arithmetic mean of the atomic electron affinity and the first ionization energy (for BiVO4, χ is 6.04 eV;[37,38] for $AgFeS_2$, χ is 5.14 eV[36]). A_f and I_1 are the atomic electron affinity and the first ionization potential, respectively. E_0 is the energy of free electrons on the hydrogen scale (about 4.5 eV), and E_g is the bandgap energy of the semiconductor. The position of the valence band edge is determined by $E_{VB} = E_{CB} + E_g$. The calculated result shows that the bottom of the conduction band of $BiVO_4$ is around 0.4 eV versus the normal hydrogen electrode (NHE), whereas the top of the valence band is around 2.7 eV. The value of E_{CB} measured (Figure S7) by photocurrent onset potential is in accordance with the calculated result. The calculated conduction band and valence band positions (vs. NHE) of $AgFeS_2$ and $BiVO_4$ are listed in Table 1.

The energy band diagram of the $AgFeS_2$–$BiVO_4$ composite photoanode is presented in Figure 9. The difference in E_{CB} between $AgFeS_2$ and $BiVO_4$ allows for the transfer of electrons from the conduction band of $AgFeS_2$ to that of $BiVO_4$. Upon light irradiation ($\lambda < 535$ nm), both the $AgFeS_2$ and $BiVO_4$ components generate electron–hole pairs, although the majority are from the $BiVO_4$ due to its large excess. Whereas the electrons are able to move easily to the FTO contact site, the holes are expected to remain on the surface of $AgFeS_2$–$BiVO_4$ photoanode. This improved charge separation efficiency leads to improved water oxidation. Conversely, under light irradiation

Table 1. Absolute electronegativity, energy band gap, calculated conduction band (CB) edge and valance band (VB) edge versus normal hydrogen electrode (NHE) at the point of zero charge for $AgFeS_2$ and $BiVO_4$ semiconductors.

Semiconductor	Abs. electroneg. (χ) [eV]	Calcd CB edge [eV]	Calcd VB edge [eV]	Energy band gap E_g [eV]
$AgFeS_2$	5.14	0.04	0.92	0.88
$BiVO_4$	6.04	0.38	2.70	2.32

beyond the absorption edge of $BiVO_4$ ($\lambda > 535$ nm), the electrons photogenerated in $AgFeS_2$ due to its small band gap can readily transfer to the conduction band of $BiVO_4$, which improves the charge carrier separation in $AgFeS_2$. $AgFeS_2$ itself is unable to directly split water toward O_2 due to the unfavorable position of the valence band with respect to the O_2/H_2O redox potential. However, the holes trapped at the $AgFeS_2$ component can react with H_2O to form OH radicals ($H_2O + h^+ \rightarrow OH^{\bullet} + H^+$).[39] OH radicals are highly reactive and, in the absence of other species, can couple with another OH radical to form H_2O_2 ($2\,OH^{\bullet} \rightarrow H_2O_2$).[40] Hydrogen peroxide is known to decompose spontaneously to O_2 and water, and H_2O_2 can also be photo-oxidized by holes in $BiVO_4$ ($H_2O_2 + h^+ \rightarrow O_2 + H^+ + 4\,e^-$).[41–43] Overall, photogenerated holes formed in both $BiVO_4$ and $AgFeS_2$, follow different pathways to react with water to form O_2. As a consequence, a higher number of collected photoelectrons are formed[44,45], which are then used for the H_2 production in the cathodic electrode.

Conclusion

Photoelectrodes made of $AgFeS_2$-nanowire–$BiVO_4$ composites were fabricated by using a facile drop-coating method. $AgFeS_2$ nanowires, with a narrow band gap of 0.9 eV, were demon-
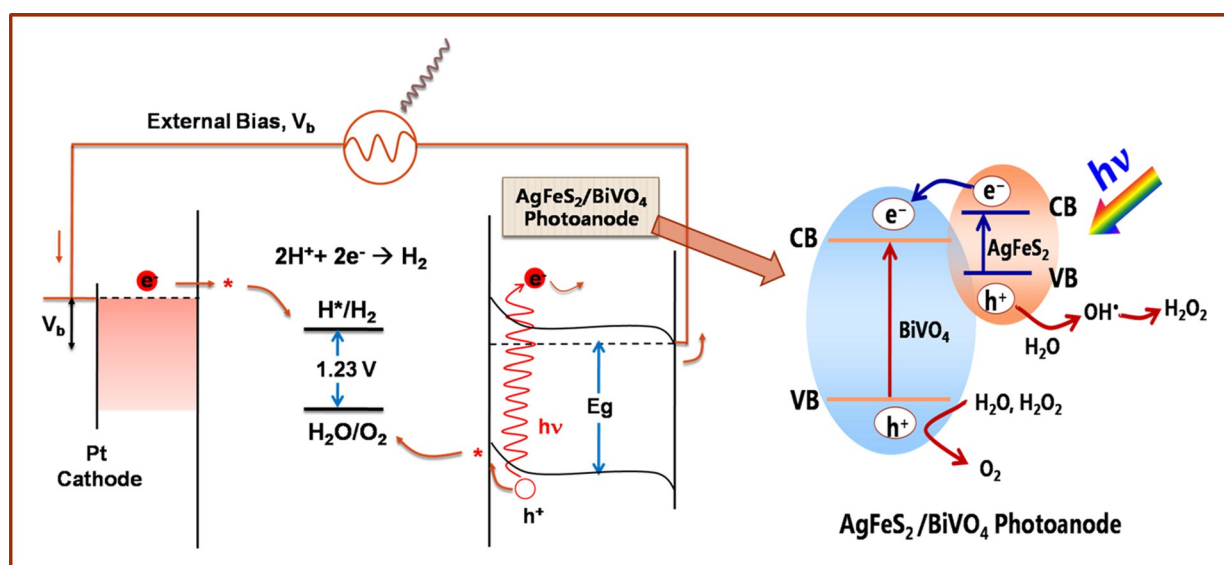
Figure 9. Mechanism of UV/Vis light absorption and charge transfer in $AgFeS_2$–$BiVO_4$ composite films for the PEC water splitting reaction.

strated as novel ternary sensitizers for improving the water splitting efficiency of a $BiVO_4$ photoanode. The photocurrent density of $AgFeS_2$–$BiVO_4$ electrode was greatly enhanced compared with pristine $BiVO_4$ electrode (15 times higher at 0.6 V vs. Ag/AgCl under AM 1.5G illumination). The excellent PEC properties arise from the extended light absorption spectrum and improved charge separation and collection efficiency. Furthermore, hydrogen and oxygen production on $AgFeS_2$–$BiVO_4$ electrodes was measured and these composite photoelectrodes were found to be promising for solar water splitting. $AgFeS_2$ drastically improves the solar water splitting efficiency of $BiVO_4$ photoanodes, suggesting $AgFeS_2$ as a new effective sensitizer for improving the efficiency of solar-to-fuel energy conversion. Further work to prepare a more active $BiVO_4$ substrate and more stable $AgFeS_2$ by surface modification is being conducted in our laboratory.

Experimental Section

Preparation of the $AgFeS_2$–$BiVO_4$ composite

The $AgFeS_2$ nanowires were obtained by using a modified synthesis from our previous report, optimized for larger scale reactions with higher yield.[25] In a typical reaction, DMSO (90 mL) was placed in a round-bottom flask and $FeCl_2$·$4H_2O$ (102 mg), thioglycolic acid (100 μL) and Ag nanowire solution (20 g L^{-1}, 2.5 mL) were added. N_2 was bubbled through the solution for 30 min to remove oxygen. Subsequently, a solution of $Na_2S_2O_3$·$5H_2O$ (451 mg) in water (10 mL) purged with N_2 was slowly added to the rest of the reagents over approximately 30 min. The color of the solution was dark purple at this stage. The flask was then placed in an oil bath at 150 °C and heated at reflux for 90 min. The solution was then allowed to cool to room temperature, centrifuged (200 g, 5 min) and washed several times in water and ethanol to remove DMSO and unreacted species. The sample was then dispersed in ethanol. A pellet of the sample was then obtained by evaporating the solvent at 50 °C.

To synthesize $BiVO_4$, $Bi(NO_3)_3$·$5H_2O$ (0.5 mmol) and NH_4VO_3 (0.5 mmol) were dissolved in nitric acid (5 mL) and distilled water (5 mL). The mixed solution (2×20 μL) was dropped onto the FTO surface of 1×1 cm area. After being dried, the film was calcined at 500 °C for 2 h with a ramping rate of 2 °C min^{-1}.

The $AgFeS_2$–$BiVO_4$ composites were prepared by dropping a suspension of $AgFeS_2$ onto the $BiVO_4$ film. Firstly, $AgFeS_2$ (4 mg) was added to ethanol (200 μL) with constant stirring. After being stirred for 24 h, the $AgFeS_2$ suspension was dropped onto the $BiVO_4$ film. The volume of $AgFeS_2$ suspension added was 10, 20, 30, 40 and 50 μL, and the corresponding $AgFeS_2$–$BiVO_4$ samples were labeled AB-10, AB-20, AB-30, AB-40 and AB-50, respectively. The $AgFeS_2$–FTO film was prepared by adding $AgFeS_2$ suspension onto a FTO film until it was fully covered.

Characterization of samples

The XRD patterns were measured on a Bruker D8 Advance X-ray diffractometer with CuKα radiation. The accelerating voltage and applied current were 40 kV and 40 mA, respectively. UV/Vis diffuse reflectance spectra of samples were collected using an UV/Vis/NIR spectrometer (UV-2600, Shimadzu co., Japan) with $BaSO_4$ as the background in the range 200–800 nm. The general morphologies

and element mapping of the products were examined by field emission scanning electron microscopy (FESEM) on a Sigma Zeiss 150 instrument (Carl Zeiss, Oberkochen, Germany) operated at 5 kV. The PEC data was collected on a CHI-660E electrochemical workstation (Chenhua Instruments, Co., Shanghai, China). The PEC experiment was performed in a conventional three-electrode system with a quartz cell. A Pt wire and an Ag/AgCl electrode were used as counter and reference electrodes, respectively. The electrolyte was Na_2SO_4 (0.1 M) solution.

Photoelectrochemical measurements

The PEC characterization was performed with the CHI-660E electrochemical workstation under illumination by a 300 W Xe lamp (CEL-S500, Beijing Jin Yuan Science and Technology Co., Beijing, China) equipped with the AM 1.5G filter (light intensity: 100 mW cm^{-2}). The incident-photon-to-current-conversion efficiency (IPCE) was measured by interposing a monochromator (7ISW15, Beijing 7-Star Optical Instruments Co., Beijing, China) between the xenon lamp and the PEC cell. The monochromatic light was passed through filter plates for different wavelengths with a bandwidth of 10 nm, and the monochromatic light power density was measured with a UV/Vis irradiatometer (CEL-NP2000, Beijing Jin Yuan science and Technology Co.) with an accuracy of 1 μW cm^{-2}.

Keywords: composite materials · extended light absorption · photoelectrochemistry · sensitizers · water splitting

[1] A. Fujishima, K. Honda, *Nature* **1972**, *238*, 37–38.
[2] L. Zhang, D. Bahnemann, *ChemSusChem* **2013**, *6*, 283–290.
[3] L. Zhang, C. Baumanis, L. Robben, T. Kandiel, D. Bahnemann, *Small* **2011**, *7*, 2714–2720.
[4] X. Zheng, D. Li, X. Li, L. Yu, P. Wang, X. Zhang, J. Fang, Y. Shao, Y. Zheng, *Phys. Chem. Chem. Phys.* **2014**, *16*, 15299–15306.
[5] X. Ba, L.-L. Yan, S. Huang, J. Yu, X.-J. Xia, Y. Yu, *J. Phys. Chem. C* **2014**, *118*, 24467–24478.
[6] Y. Park, K. J. McDonald, K. S. Choi, *Chem. Soc. Rev.* **2013**, *42*, 2321–2337.
[7] A. Kudo, K. Ueda, H. Kato, I. Mikami, *Catal. Lett.* **1998**, *53*, 229–230.
[8] A. Kudo, K. Omori, H. Kato, *J. Am. Chem. Soc.* **1999**, *121*, 11459–11467.
[9] F. F. Abdi, L. Han, A. H. Smets, M. Zeman, B. Dam, R. van de Krol, *Nat. Commun.* **2013**, *4*, 2195.
[10] H. Ye, J. Lee, J. S. Jang, A. J. Bard, *J. Phys. Chem. C* **2010**, *114*, 13322–13328.
[11] C. Li, P. Zhang, R. Lv, J. Lu, T. Wang, S. Wang, H. Wang, J. Gong, *Small* **2013**, *9*, 3951–3956.
[12] Y. Hu, D. Li, Y. Zheng, W. Chen, Y. He, Y. Shao, X. Fu, G. Xiao, *Appl. Catal. B* **2011**, *104*, 30–36.
[13] L. Zhang, C.-Y. Lin, V. K. Valev, E. Reisner, U. Steiner, J. J. Baumberg, *Small* **2014**, *10*, 3970–3978.

[14] L. Zhang, E. Reisner, J. J. Baumberg, *Energy Environ. Sci.* **2014**, *7*, 1402–1408.

[15] W. Luo, Z. Yang, Z. Li, J. Zhang, J. Liu, Z. Zhao, Z. Wang, S. Yan, T. Yu, Z. Zou, *Energy Environ. Sci.* **2011**, *4*, 4046–4051.

[16] K. J. McDonald, K.-S. Choi, *Energy Environ. Sci.* **2012**, *5*, 8553–8557.

[17] Y. Liang, T. Tsubota, L. P. A. Mooij, R. van de Krol, *J. Phys. Chem. C* **2011**, *115*, 17594–17598.

[18] W. J. Jo, J.-W. Jang, K.-j. Kong, H. J. Kang, J. Y. Kim, H. Jun, K. P. S. Parmar, J. S. Lee, *Angew. Chem. Int. Ed.* **2012**, *51*, 3147–3151; *Angew. Chem.* **2012**, *124*, 3201–3205.

[19] K. P. S. Parmar, H. J. Kang, A. Bist, P. Dua, J. S. Jang, J. S. Lee, *ChemSusChem* **2012**, *5*, 1926–1934.

[20] D. K. Zhong, S. Choi, D. R. Gamelin, *J. Am. Chem. Soc.* **2011**, *133*, 18370–18377.

[21] S. K. Pilli, T. G. Deutsch, T. E. Furtak, J. A. Turner, L. D. Brown, A. M. Herring, *Phys. Chem. Chem. Phys.* **2012**, *14*, 7032–7039.

[22] S. Kohtani, J. Hiro, N. Yamamoto, A. Kudo, K. Tokumura, R. Nakagaki, *Catal. Commun.* **2005**, *6*, 185–189.

[23] H.-q. Jiang, H. Endo, H. Natori, M. Nagai, K. Kobayashi, *Mater. Res. Bull.* **2009**, *44*, 700–706.

[24] L. Yu, R. S. Kokenyesi, D. A. Keszler, A. Zunger, *Adv. Energy Mater.* **2013**, *3*, 43–48.

[25] B. Sciacca, A. O. Yalcin, E. C. Garnett, *J. Am. Chem. Soc.* **2015**, *137*, 4340–4343.

[26] S. K. Han, C. Gu, M. Gong, Z.-M. Wang, S.-H. Yu, *Small* **2013**, *9*, 3765–3769.

[27] M. Zhou, J. Bao, Y. Xu, J. Zhang, J. Xie, M. Guan, C. Wang, L. Wen, Y. Lei, Y. Xie, *ACS Nano* **2014**, *8*, 7088–7098.

[28] M. A. Butler, *J. Appl. Phys.* **1977**, *48*, 1914–1920.

[29] Y. Park, K. J. McDonald, K. S. Choi, *Chem. Soc. Rev.* **2013**, *42*, 2321–2337.

[30] C. Martinez Suarez, S. Hernández, N. Russo, *Appl. Catal. A* **2015**, *504*, 158–170.

[31] J. Wang, P. Wang, Y. Cao, J. Chen, W. Li, Y. Shao, Y. Zheng, D. Li, *Appl. Catal. B* **2013**, *136–137*, 94–102.

[32] A. Hagfeldt, H. Lindström, S. Södergren, S.-E. Lindquist, *J. Electroanal. Chem.* **1995**, *381*, 39–46.

[33] N. J. Bell, Y. H. Ng, A. Du, H. Coster, S. C. Smith, R. Amal, *J. Phys. Chem. C* **2011**, *115*, 6004–6009.

[34] X. Yang, A. Wolcott, G. Wang, A. Sobo, R. C. Fitzmorris, F. Qian, J. Z. Zhang, Y. Li, *Nano lett.* **2009**, *9*, 2331–2336.

[35] A. Murphy, P. Barnes, L. Randeniya, I. Plumb, I. Grey, M. Horne, J. Glasscock, *Int. J. Hydrogen Energy* **2006**, *31*, 1999–2017.

[36] Y. Xu, M. A. A. Schoonen, *Am. Mineral.* **2000**, *85*, 543–556.

[37] M. Long, W. Cai, J. Cai, B. Zhou, X. Chai, Y. Wu, *J. Phys. Chem. B* **2006**, *110*, 20211–20216.

[38] M. A. Butler, *J. Electrochem. Soc.* **1978**, *125*, 228.

[39] D. Hidalgo, S. Bocchini, M. Fontana, G. Saracco, S. Hernández, *RSC Adv.* **2015**, *5*, 49429–49438.

[40] P. Akhter, M. Hussain, G. Saracco, N. Russo, *Fuel* **2015**, *149*, 55–65.

[41] J. R. Harbour, J. Tromp, M. L. Hair, *Can. J. Chem.* **1985**, *63*, 204–208.

[42] B. Jenny, P. Pichat, *Langmuir* **1991**, *7*, 947–954.

[43] I. Ilisz, K. Föglein, A. Dombi, *J. Mol. Catal. A: Chem.* **1998**, *135*, 55–61.

[44] A. Lamberti, A. Sacco, D. Hidalgo, S. Bianco, D. Manfredi, M. Quaglio, E. Tresso, C. F. Pirri, *Acta Phys. Pol. A* **2013**, *123*, 376–379.

[45] S. Hernández, V. Cauda, A. Chiodoni, S. Dallorto, A. Sacco, D. Hidalgo, E. Celasco, C. F. Pirri, *ACS Appl. Mater. Interfaces* **2014**, *6*, 12153–12167.